

accepted by the Astronomical Journal

Intergalactic HII Regions Discovered in SINGG

E. V. Ryan-Weber^{1,2}, G. R. Meurer³, K. C. Freeman⁴, M. E. Putman⁵, R. L. Webster¹, M. J. Drinkwater⁶, H. C. Ferguson⁷, D. Hanish³, T. M. Heckman³, R. C. Kennicutt, Jr.⁸, V. A. Kilborn⁹, P. M. Knezek¹⁰, B. S. Koribalski², M. J. Meyer¹, M. S. Oey¹¹, R. C. Smith¹², L. Staveley-Smith², and M. A. Zwaan¹

ABSTRACT

A number of very small isolated HII regions have been discovered at projected distances up to 30 kpc from their nearest galaxy. These HII regions appear as tiny emission line objects in narrow band images obtained by the NOAO Survey for Ionization in Neutral Gas Galaxies (SINGG). We present spectroscopic confirmation of four isolated HII regions in two systems, both systems have tidal HI features. The results are consistent with stars forming in interactive debris due to cloud-cloud collisions. The H α luminosities of the isolated HII regions are equivalent to the ionizing flux of only a few O stars each. They are most likely ionized by stars formed in situ, and represent atypical star formation in the low density environment of the outer parts of galaxies. A small but finite intergalactic star formation rate will enrich and ionize the surrounding medium. In one system, NGC 1533, we calculate a star formation rate of $1.5 \times 10^{-3} M_{\odot} \text{yr}^{-1}$, resulting in a metal enrichment of $\sim 1 \times 10^{-3}$ solar for the continuous formation of stars. Such systems may have been more common in the past and a similar enrichment level is measured for the ‘metallicity floor’ in damped Lyman- α absorption systems.

¹School of Physics, University of Melbourne, VIC 3010, Australia.

²Australia Telescope National Facility, CSIRO, P.O. Box 76, Epping, NSW 1710, Australia.

³Department of Physics and Astronomy, The Johns Hopkins University, Baltimore, MD 21218-2686, USA

⁴Research School of Astronomy & Astrophysics, Mount Stromlo Observatory, Cotter Road, Weston, ACT 2611, Australia.

⁵CASA, University of Colorado, Boulder, CO 80309-0389, USA.

⁶Department of Physics, University of Queensland, Brisbane, Queensland, 4072, Australia

⁷Space Telescope Science Institute, 3700 San Martin Drive, Baltimore, MD 21218, USA

⁸Steward Observatory, University of Arizona, Tuscon, AZ 85721, USA

⁹Jodrell Bank Observatory, University of Manchester, Macclesfield, Cheshire, SK11 9DL, U.K.

¹⁰WIYN Observatory, 950 N. Cherry Avenue, Tuscon, AZ 85719, USA

¹¹Lowell Observatory, 1400 West Mars Hill Rd, USA

¹²Cerro Tololo Inter-American Observatory, Casilla 603, Chile

Subject headings: HII regions — stars: formation — galaxies: halos — intergalactic medium — galaxies: star clusters

1. Introduction

H II regions signifying the presence of highly ionizing OB stars are usually found in the luminous inner regions of galaxies (e.g. Martin & Kennicutt 2001). H II regions are also located in the faint outer arms of spirals (e.g. Ferguson et al. 1998b), and as single or multiple star forming knots in narrow emission line dwarfs (H II galaxies). In each case, new stars are formed in the vicinity of an existing stellar population. However, recent observations by Gerhard et al. (2002) have spectroscopically confirmed an isolated compact H II region on the extreme outskirts of a galaxy (NGC 4388) in the Virgo cluster. Several luminous H α -emitting knots have also been discovered in a compact group in the A1367 cluster (Sakai et al. 2002). In these cases it appears that the H II regions are due to newly formed stars where no stars existed previously, albeit in a galaxy cluster environment.

As they evolve, OB stars increase the metal abundance in their local environment. Absorption line studies show that the intergalactic medium (IGM) and galaxy halos, including our own, are enriched (e.g. Chen et al. 2001; Tripp et al. 2002; Collins et al. 2003). Isolated H II regions provide a potential source for this enrichment. In situ star formation in the IGM offers an alternative to galactic wind models to explain metal enrichment hundreds of kilo-parsecs from the nearest galaxy.

Here we present a number of very small isolated H II regions that have been discovered by their H α emission in the narrow band images obtained by the NOAO Survey for Ionization in Neutral Gas Galaxies (SINGG). SINGG is an H α survey of an H I-selected sample of nearby galaxies. The survey is composed of nearly 500 galaxies from the H I Parkes All-Sky Survey (HIPASS, Barnes et al. 2001; Meyer et al. 2003), of these about 300 have been observed in H α . Since a gaseous reservoir is a prerequisite for star formation, SINGG measures a broad census of star formation in the local Universe. The H II regions appear as tiny emission line objects at projected distances up to 30 kpc from the apparent host galaxy. H II regions are defined as isolated when they are projected at least twice the $\mu_R = 25$ mag arcsec $^{-2}$ isophotal radius from the apparent host galaxy. This is typically much further than outer disk H II regions in spiral galaxies (Ferguson et al. 1998b). In fact, for the systems discussed in detail here it is not totally clear whether the isolated H II regions are even bound to the apparent host, hence we refer to them as “intergalactic”. Their high equivalent widths suggest they are due to newly formed stars where no stars existed previously.

In Section 2 spectra is presented for five isolated H II regions candidates in three systems. These five candidates are referred to as the spectroscopically *detected* emission line objects or H II region candidates. All but one source has H α detected at a comparable recessional velocity to the nearest galaxy, two sources are also detected in [O III] as further confirmation. These four objects are referred to as the spectroscopically *confirmed* isolated H II regions. Optical spectra and

H_I distributions for all three systems are described in Sections 3–5. In Section 6 models of the underlying stellar population, scenarios for star formation, enrichment of the IGM, implications of the intergalactic star formation rate, and the possibility that isolated H_{II} regions are progenitors of tidal dwarf galaxies are discussed. $H_0 = 75 \text{ km s}^{-1}\text{Mpc}^{-1}$ is used throughout.

2. Observations

Continuum R-band and narrow band H_α images of local gas-rich galaxies were taken with the CTIO 1.5m telescope as part of SINGG. At least three images were taken in each band, with small ($\lesssim 1'$) dithers between images. Each image was processed through overscan and bias subtraction, followed by division by a flatfield derived from both dome and twilight sky flats. The images in each band were aligned and combined. The R or narrow-band image with the better seeing was convolved to match the poorer seeing of the other image, and then the R image was scaled and subtracted from the narrow band image to produce a net H_α image. The final images have a pixel scale of 0.43'' per pixel and subtend a field of view of nearly 15''. The properties of the SINGG images are given in Table 1. The Table includes the 5σ point source detection limit and the large scale surface brightness limit for both R & H_α images. The latter was determined from the rms variation in the mean background level determined in boxes 35 pixels on a side after iteratively clipping pixels that deviate by more than 5 times the pixel to pixel rms from each box. The box to box variation of the mean is less than 1% of the sky level in all cases.

The candidate isolated H_{II} regions were identified as unresolved high equivalent width (EW) sources outside the optical disk of each galaxy. Individual exposures were checked and candidates with sharp edges (likely due to cosmic ray residuals) or bright continua were rejected. Aperture photometry was performed on each of the isolated H_{II} regions in the flux calibrated SINGG images using *idlastro* routines in IDL yielding H_α and R fluxes. Since the H_{II} regions have high equivalent widths, the R count rates were corrected for H_α line emission using the formula

$$C'_R = C_R - \frac{T_R(\lambda)}{T_{NB}(\lambda)} * C_{H\alpha} \quad (1)$$

where C'_R is the corrected R count rate, C_R and $C_{H\alpha}$ are the measured count rates in the R and net H_α image, and $T_R(\lambda)$ and $T_{NB}(\lambda)$ are the throughputs of the filter evaluated at the wavelength λ of H_α. For the spectroscopically detected cases, λ was taken from the spectra; otherwise we assumed that SINGG was detecting net H_α emission redshifted by the H_I heliocentric radial velocity. The results are given in Table 2. The spectroscopically detected isolated H_{II} regions have H_α fluxes in the range 6.9 to $11 \times 10^{-16} \text{ erg s}^{-1}\text{cm}^{-2}$. Assuming the distance to each isolated H_{II} regions is the same as the host galaxy in each system, the H_α luminosities are $4\pi D^2 f_{H\alpha} = 3.5 \times 10^{36}$ to $3.5 \times 10^{38} \text{ erg s}^{-1}$. In most cases the isolated H_{II} regions are barely detected in continuum emission in the SINGG R images with a typical 5σ detection limit of around $1 \times 10^{-18} \text{ erg s}^{-1}\text{cm}^{-2}\text{\AA}^{-1}$ (see Tables 1 and 2). Isophotal radii at $\mu_R = 25\text{mag arcsec}^{-2}$ were measured for each galaxy using the

ellipse task in IRAF. The galaxy-H II region separations are given as a function of these radii in Table 3.

Spectra of 11 isolated H II region candidates were obtained with the double beam spectrograph (DBS) on the RSAA 2.3m telescope in September 2002. Due to the very low continuum flux of the emission line objects, it was necessary to use a nearby star to align the slit on each H II region candidate in the DBS auto-guider. Three 2000 second exposures were taken of each object. The spectra were reduced using standard procedures in IRAF. The dispersion of the red spectra (6000 - 7000 Å) was 0.55 Å per pixel, corresponding to a resolution of 1.1 Å per pixel or 50 km s⁻¹. The dispersion of the blue spectra (3500 - 5400 Å) was 1.1 Å per pixel, corresponding to a resolution of 2.2 Å per pixel or 150 km s⁻¹. An additional two exposures of the candidate H II region near ESO 149-G003 were obtained in October 2003 using the same DBS set-up. These additional exposures have been combined with the first spectra to give the result in Figure 1.

Five of the 11 observed isolated H II region candidates were detected. The non-detected candidates mostly have $F_{\text{H}\alpha} < 4 \times 10^{-16}$ erg cm⁻² s⁻¹ (with the exception of the candidate H II region near NGC 1314) and have a range of continuum fluxes. In each case the DBS red spectrum fully covers the narrow band SINGG filter range. Since the spectra do not confirm the reality of these 6 isolated H II region candidates, they will not be discussed further. Four of the 5 detected isolated H II regions have confirmed emission lines within the narrow band filter's passband close to the expected position of H α (6563 Å) at recessional velocities close to that of their respective host galaxies (measured from HIPASS, see Table 3, column 2). The recessional velocity measured from each H α line is given in Table 2. Some isolated H II regions were also detected in [O III] (5007 Å), confirming that the emission seen in the SINGG images is indeed H α . The presence of both H α and [O III] lines in these cases places the isolated H II regions at comparable recessional velocities to the galaxy (or galaxies) in each field, and rules out the possibility that they are background emission line systems. Spectra for the 5 detected isolated H II regions are given in Figure 1. The H α spectra (red arm) have been normalised by the continuum subtracted H α fluxes from the SINGG images. The H α line fluxes have not been corrected for [N II] contamination. For the FWHM \sim 35Å filters used in this study we expect the combined [N II] 6548+6583 contamination to be <10% if the line flux ratio [N II] 6548/H α = 0.35. The [O III] line lies in the blue arm and the flux calibration of the spectra is uncertain. Details of the 3 systems, which include the 5 spectroscopically detected isolated H II regions, are discussed in the next section.

In addition to the H α images and spectra, Australia Telescope Compact Array (ATCA) H I maps are available for two systems, NGC 1533 and ESO 149-G003. The ATCA data reduction is detailed in Ryan-Weber et al. (2003b). The two datasets have a restored beam of 68'' \times 65'' and 79'' \times 61'' respectively. The velocity resolution is 3.3 km s⁻¹ and the RMS noise is 3.7 mJy beam⁻¹ per channel, corresponding to a 3 σ column density limit (over a line width of 40 km s⁻¹) of 3.2×10^{19} cm⁻².

3. Three Systems with Detected Isolated H_{II} regions

3.1. NGC 1533

Figure 2 shows a DSS image of NGC 1533 overlaid with ATCA H_I contours. The insert has the same contours overlaid on the H_α image with the isolated H_{II} regions labelled. The H_I distribution around NGC 1533 consists of two major arcs, the NW cloud and the SE cloud. H_I gas with column densities below the lowest contour close the H_I in a ring. No obvious optical counterpart to this ring is seen in the DSS nor R SINGG image. The total H_I mass of the system (based on the total flux density from HIPASS of $67.6 \text{ Jy beam}^{-1} \text{km s}^{-1}$) is $7 \times 10^9 \text{ M}_\odot$. The SE cloud contains $\sim \frac{1}{3}$ of this total H_I mass ($2.4 \times 10^9 \text{ M}_\odot$). The projected distance between the H_I arcs and the optical centre of NGC 1533 ranges from $2'$ to $11.7'$, corresponding to a projected physical length between 12 and 70 kpc.

NGC 1533 is an S0 galaxy located 1° from the center of the Dorado group. The two smaller galaxies in the NW corner of the image are IC 2039 (closest to NGC 1533, uncertain redshift, no H_I detected) & IC 2038 (contains associated H_I). The peculiar distribution of H_I is thought to arise from the destruction of a galaxy to form a tidal remnant around NGC 1533. If the H_I was stripped from IC2038/9, these galaxies would need to account for all the H_I in the system and therefore have $M_{\text{HI}}\text{-to-}L_B$ ratios greater than 15, which is not very likely for their morphologies. The progenitor is more likely a low surface brightness (LSB) galaxy with a moderate H_I mass, whose optical counterpart is now too diffuse to identify. N-body/SPH numerical simulations showing the orbital evolution of a LSB galaxy in NGC 1533's gravitational potential support this hypothesis (Ryan-Weber et al. 2003a).

The velocities of the three confirmed isolated H_{II} regions (1, 2 and 5), 846, 831 and 901 km s⁻¹, compare well with the velocity of NGC 1533 at 785 km s⁻¹ and lie within the range of H_I velocities in the SE cloud (883 km s⁻¹ with a width at 50% peak, $w_{50} = 71 \text{ km s}^{-1}$). Interestingly, the isolated H_{II} regions do not appear to be correlated with the densest regions of H_I and are located in the SE cloud only. At this resolution (~ 6 kpc) the densest region of H_I is the central part of the NW cloud. The stellar concentrations of tidal dwarf galaxies are located in the densest regions of H_I, mapped in 21-cm at similar resolutions (~ 4 kpc, e.g. Duc et al. 2000). Furthermore, the H_I in the SE cloud has velocity dispersions up to 30 km s⁻¹ and velocity gradients in the range 7-50 km s⁻¹ kpc⁻¹, making it an unlikely site for star formation. Star formation usually requires the gas to have a low velocity dispersion in order to collapse gravitationally.

3.2. HCG 16

The isolated H_{II} region in the compact group HCG 16, shown in Figure 3, is near the two galaxies NGC 835 (SBab) and NGC 833 (Sa). The velocity of the isolated H_{II} region (3634 km s^{-1}) sits on the lower edge of the H_I emission measured by HIPASS (velocity = 3917 km s^{-1} , $w_{50} =$

288 km s^{-1} , $w_{20} = 391 \text{ km s}^{-1}$) and below the optical velocities of NGC 835 and NGC 833 (4073 and 3864 km s^{-1} respectively, from NASA/IPAC Extragalactic Database, NED). The 2D spectrum shows the $\text{H}\alpha$ emission line from NGC 833 at 3864 km s^{-1} and diffuse emission decreasing in velocity to $\sim 3700 \text{ km s}^{-1}$ half way along the line towards the isolated H II region. Verdes-Montenegro et al. (2001) have published a VLA map of HCG 16, showing H I in NGC 835 and 833 with a large tidal feature to the NE (overlapping the isolated H II region position) that joins other group members several arcminutes away to the east.

3.3. ESO 149-G003

The velocity of the isolated H II region candidate near the irregular galaxy ESO 149-G003 (949 km s^{-1}) is quite offset from its apparent host galaxy (H I velocity of 576 km s^{-1} and $w_{50} = 39 \text{ km s}^{-1}$). The long-slit spectrum of the H II region candidate also includes the southern part of the galaxy, and the galaxy $\text{H}\alpha$ emission line has a measured velocity of $628 \pm 50 \text{ km s}^{-1}$. This 52 km s^{-1} deviation, just inside the quoted uncertainty, could be due to the slit being aligned along the southern part of the galaxy only, although the H I spectrum does not show a large velocity gradient. A velocity difference of 321 km s^{-1} is measured between the galaxy and H II region candidate optical emission lines, assuming the single emission line is indeed $\text{H}\alpha$. The narrow H I profile shows no anomalous velocity gas. Follow-up ATCA observations show no H I emission at the velocity and position of the emission line object to $M_{\text{HI}} \leq 8 \times 10^5$ (3×10^6) M_{\odot} at a 3σ limit, and assuming a distance of 6.5 (12) Mpc. ESO 149-G003 seems quite isolated, and the nearest galaxy in both NED and HIPASS (Meyer et al. 2003) is ESO 149-G013 at 1500 km s^{-1} , 1.6° ($\sim 560 \text{ kpc}$) away. However, ESO 149-G003 does show signs of a flared or warped optical disk at the edges, suggesting an interaction has taken place (see Figure 4). A strong positive correlation between warping in late-type galaxies and environment (Reshetnikov & Combes 1998) has been largely attributed to tidal interactions. However, since only one emission line ($\text{H}\alpha$) is detected in this case, the possibility that this candidate isolated H II region is a background emission line source cannot be ruled out, for example $\text{H}\beta$ at $z \sim 0.4$ or $[\text{O III}]$ at $z \sim 0.3$.

4. Discussion

4.1. Underlying Stellar Population

The $\text{H}\alpha$ luminosities of the detected isolated H II regions (3.5×10^{36} to $3.5 \times 10^{38} \text{ erg s}^{-1}$) place them at the low luminosity end of the H II region luminosity function (e.g. Oey & Clarke 1998). The $\text{H}\alpha$ -luminosity of an H II region is proportional to the ionizing photon luminosity (Q_0) above the Lyman limit (912 Å) from nearby stars. From equation 5.23 in Osterbrock (1989), $Q_0 = (\alpha_B / \alpha_{H\alpha}^{eff}) \times (L_{H\alpha} / E_{H\alpha}) = 7.33 \times 10^{11} L_{H\alpha}$, and using the ionizing luminosity of an O5V star (Vacca et al. 1996), each isolated H II region is illuminated by the equivalent of 0.1 – 8 O5V stars

each. The least luminous detected isolated H II region can be ionized by a single O9.5 star.

The underlying stellar population is very weak in most of the spectroscopically detected emission line objects, in two of the five cases it is undetected in the SINGG images. This makes it difficult to constrain whether the isolated H II regions are ionized by a single isolated massive star, or whether the massive star or stars represent the ‘tip of the iceberg’ of a cluster. A single massive star could have formed spontaneously; examples of this exist in the disk of the Milky Way, where IR observations show an isolated massive star (Ballantyne et al. 2000). However, most massive stars form as part of a cluster (Clarke et al. 2000), with a characteristic Initial Mass Function (IMF). The very low continuum emission does rule out a significant underlying stellar population and suggests that isolated H II regions are due to newly formed clusters where no stars existed previously. The low continuum emission also separates isolated H II regions from H II galaxies and tidal dwarf galaxies. Three of the four confirmed isolated H II regions have $\text{EW}(\text{H}\alpha) > 1000 \text{ \AA}$. By comparison, H II regions in the outer arms of spiral galaxies (beyond the B 25th-magnitude isophote) measured by Ferguson et al. (1998a) have an average $\text{EW}(\text{H}\alpha) = 364 \text{ \AA}$. Furthermore, most of the group of star forming dwarf galaxies in A1367 have $\text{EW}(\text{H}\alpha) < 100 \text{ \AA}$ (Sakai et al. 2002).

Upper limit estimates of the underlying stellar population can be obtained from star formation models, such as Starburst99 (Leitherer et al. 1999). The ratio of Q_0 to the continuum luminosity, L_v , can be used to find the age of the population. Since very little continuum emission is detected from the isolated H II regions, the ratio Q_0/L_v is large, suggesting a very young age, in the range 3 to 7×10^6 years, for the parameters of the five detected H I regions. Indeed young ages are expected since we selected isolated H II region candidates with high equivalent widths. Using the Starburst99 model with a Salpeter IMF, $M_{up} = 100 \text{ M}_\odot$, and metallicity of 0.4 solar, a very young instantaneous burst is predicted to have a photon luminosity in the range $\log Q_0 = 51.3$ to $52.7 \text{ photons sec}^{-1}$ for a system with 10^6 M_\odot . The same model predicts 1.2 to 4.5×10^3 O stars (in the spectral range O3 to O9.5). Scaling Q_0 with $Q_0(\text{H II region})$ the number of O stars ionizing each isolated H II region is in the range 4 – 7, corresponding to a total cluster mass of $0.9 - 1.8 \times 10^3 \text{ M}_\odot$. The HCG 16 isolated H II region is significantly more luminous in H α , according to this model, it would consist of 23 O stars in a cluster of $5 \times 10^3 \text{ M}_\odot$. The ESO 149-G003 isolated H II region, unlike the others, does have considerable continuum emission in the R image (see Table 2). This suggests a slightly older population (7×10^6 years) with 1.4 O stars and cluster mass of $1.2 \times 10^3 \text{ M}_\odot$. These models account for the nebula emission in the continuum luminosity.

Continuous star formation models predict stellar population ages in the range 6×10^6 to 1.5×10^7 years for isolated H II regions with the largest equivalent widths (HCG 16 1, NGC 1533 1 & 5). In these cases, the calculated ages are consistent with the instantaneous burst models, and confirm that the isolated H II regions are due to newly formed clusters where no stars existed previously. A stellar age of 3×10^8 years is found for a continuous star formation model of NGC 1533 2. The low equivalent width of the candidate H II region in the ESO 149-G003 field however cannot be reasonably fit by the continuous star formation models.

The calculations above assumes a simple scaling of the number of ionizing stars with total cluster mass. At small cluster masses, the differences between analytic and stochastic IMFs can be substantial, especially in the number of high mass stars. Statistical errors in stellar population models are discussed by Cerviño et al. (2002). Monte Carlo simulations can be used to investigate the effects of small initial masses on clusters. Garcia Vargas & Diaz (1994) found the probability of finding a small cluster with an $M > 60 M_{\odot}$ star is not zero, as suggested by the analytic IMF, but rises to 12%. Monte Carlo simulations by Cerviño & Mas-Hesse (1994) also obtain similar results. These simulations suggest that the total cluster mass calculated above could be overestimated.

4.2. Origins of Isolated H II Regions

Since we have just two systems with confirmed isolated H II regions it is difficult to draw any conclusions on a common formation scenario, if one exists. Evidence of interactions, however, feature in all systems. NGC 1533 and HCG 16 both display tidally disrupted H I outside the main optical region of the galaxies. Although the isolated H II region projected to be near ESO 149-G003 could be a background object, if the two are associated, the warping in ESO 149-G003’s disk could indicate an interaction has occurred. The two systems that feature similar objects reported in the literature, NGC 4388 in the Virgo cluster (Vollmer & Huchtmeier 2003; Gerhard et al. 2002) and A1367 (Sakai et al. 2002), also show disrupted H I. Vollmer & Huchtmeier (2003) use ram pressure stripping to explain the isolated H II region near NGC 4388. Ram pressure stripping is less likely in our two systems, which occur in much less dense environments.

The projected separations between the isolated H II regions and host galaxies (see Table 3) suggest the underlying massive stars have mostly likely formed in situ. Alternatively, the stars could have formed in the galaxy and then been ejected. Typical ejection velocities due to dynamical interactions do not exceed 200–300 km s^{−1} (Leonard & Duncan 1988). However the velocity required to travel 4–33 kpc in the lifetime of a massive star ($\sim 10^7$ yrs) is 390–3200 km s^{−1}. The close match in velocity between the isolated H II regions and galaxy, at least in the NGC 1533 system, suggest that the isolated H II regions are not currently moving at a high relative speed.

Our own Galactic halo has interactive H I debris which appears to be forming stars. The Magellanic Bridge is an H I complex that joins the Large and Small Magellanic Clouds at ~ 50 kpc and represents the interaction between these two galaxies (e.g. Putman et al. 2003). Simulations indicate the Bridge was formed 200 – 500 Myr ago (e.g. Gardiner & Noguchi 1996), but the stars in the Bridge are between 10 – 25 Myr old (e.g. Demers & Battinelli 1998), indicating that star formation is currently active within this gas-dominated tidal feature.

We have three confirmed isolated H II regions with detailed H I information in the NGC 1533 system. The high velocity dispersions and gradients in the vicinity of the isolated H II regions in this system suggest that star formation is not occurring via the usual gravitational collapse methods. Star formation could be shock-induced by clouds colliding (e.g. Zhang et al. 2001; Sato et al. 2000).

Is it reasonable to expect collisions in the NGC 1533 system? Christodoulou et al. (1997) calculated the timescale for collisions in low density environments such as Galactic HVCs and the Magellanic Stream and Bridge. Following Christodoulou et al. (1997), a cloud on a random walk with velocity dispersion σ_v , has a characteristic time between collisions of $\tau_1 = l/\sigma_v$, where the mean free path $l = V/(N\pi R^2)$, that is the volume (V) divided by the number of clouds (N) with cross section πR^2 . Considering all clouds in the volume, the characteristic time between any two collision is $\tau_c = \tau_1/N = V/(N^2\pi R^2\sigma_v)$.

The H I ring around NGC 1533 appears to be clumped on scales of no greater than the resolution of the image ($\sim 1'$), corresponding to a radius of 3 kpc at a distance of 21 Mpc. Of course, the gas is likely to be clumped on smaller scales too, so this radius is an upper limit. The density, ρ , can be estimated from the surface density, N_{HI} , where $\rho = m_H N_{\text{HI}}/(2R) = 1.8 \times 10^{-26} \text{ g cm}^{-3}$. The mass of each cloud is then given by $M_{\text{HI}} = 4\pi\rho R^3/3 = 3.0 \times 10^7 M_{\odot}$. Since the entire ring has an H I mass of $7 \times 10^9 M_{\odot}$, it could be composed of 200 such clouds. The total ring surface area covered by H I with column densities greater than $2 \times 10^{20} \text{ cm}^{-2}$ is $4 \times 10^3 \text{ kpc}^2$, assuming a thickness of at least a cloud diameter (6 kpc), gives a volume estimate of $24 \times 10^3 \text{ kpc}^3$. The velocity dispersion in the ring varies from 5 km s^{-1} in the NW part to 30 km s^{-1} in the SE. The timescale of a collision between any two clouds is therefore,

$$\tau_c = 6.9 \times 10^5 \left(\frac{V}{24 \times 10^3 \text{ kpc}^3} \right) \left(\frac{N}{200} \right)^{-2} \left(\frac{R}{3 \text{ kpc}} \right)^{-2} \left(\frac{\sigma_v}{30 \text{ km s}^{-1}} \right)^{-1} \text{ yr.} \quad (2)$$

This timescale varies between $1 - 4 \times 10^6$ yrs depending on σ_v (and is a lower limit for smaller cloud radii). The lifetime of an O star is only 1×10^7 yrs, so we would expect to see 2 – 14 star formation events due to cloud collisions at any one time. This estimate agrees with the fact we see 5 isolated H II regions in the NGC 1533 ring. This formation scenario is therefore plausible.

4.3. IGM Enrichment

Although the H α luminosities are small, an estimate of the star formation rate can be obtained by the relation $\text{SFR} (M_{\odot}\text{yr}^{-1}) = L_{H\alpha}/1.26 \times 10^{41} \text{ erg s}^{-1}$ (Kennicutt 1998). Summing the H α luminosities from the 5 isolated H II regions in the NGC 1533 system, the $\text{SFR} = 1.5 \times 10^{-3} M_{\odot}\text{yr}^{-1}$. The other systems with only one isolated H II region are lower still. A small, but finite intergalactic star formation rate will continually enrich and ionize the IGM. Maeder (1992) calculated the total yield (y) of metals expelled in winds and ejecta from supernova and planetary nebula. For a Salpeter IMF and a range of initial metallicities, they find $0.022 < y < 0.027$. Therefore a $\text{SFR} = 1.5 \times 10^{-3} M_{\odot}\text{yr}^{-1}$ will return $\sim 4 \times 10^{-5} M_{\odot}\text{yr}^{-1}$ of metals into the surrounding medium. Simulations of the dynamical evolution of H I gas around NGC 1533 show that it could last up to 1 Gyr (Ryan-Weber et al. 2003a). This is considered an upper limit since no consumption of gas due to the formation of stars is taken into account. If the SFR is maintained for 1 Gyr, metals will pollute the $2.4 \times 10^9 M_{\odot}$ of H I in the SE cloud, resulting in a metallicity of $\sim 1 \times 10^{-3}$ solar. Alternatively if the SFR

was not continuous and corresponded to a single population of stars only, the resulting metallicity would be negligible ($\sim 1 \times 10^{-6}$ solar).

How does this compare to the abundances seen in Ly α absorption line systems? H I in the vicinity of the NGC 1533 isolated H II regions has $N_{\text{HI}} = 1 - 4 \times 10^{20} \text{ cm}^{-2}$, equivalent to a damped Ly α absorption (DLA, $N_{\text{HI}} \geq 2 \times 10^{20} \text{ cm}^{-2}$) or sub-DLA system ($10^{19} < N_{\text{HI}} < 2 \times 10^{20} \text{ cm}^{-2}$). The metallicity of DLA or sub-DLA gas at low redshift varies from 0.01 solar (e.g I Zw 18 Aloisi et al. 2003) to solar. Depending on the initial metallicity, the isolated H II regions would enrich the NGC 1533 system by 10 percent at the most. At higher redshifts however, this increase in metallicity could be more significant. (Prochaska et al. 2003) find a DLA ‘metallicity floor’ at $\sim 1.4 \times 10^{-3}$ solar, over a redshift range from 0.5 to 5. Intergalactic star formation may have contributed to this. DLAs with larger velocity widths are found to have higher metallicities (Nestor et al. 2003), this trend is also hinted upon in the sub-DLA data (Peroux et al. 2003). Larger velocity widths may indicate interacting systems. In addition, since collisions and tidal disruptions of galaxies were more common at higher redshifts, the amount of high N_{HI} -gas outside galaxies was greater and therefore the intergalactic star formation rate could have been higher in the past.

4.4. Kinematics and the Tidal Dwarf Galaxy Connection

Comparing the velocity of isolated H II regions to their apparent host galaxy and associated H I gas is useful in determining their dynamical connection. In Figure 5 the H I spectrum for each system is plotted with the velocity of the detected emission line objects, assuming the line is indeed H α . For the NGC 1533 system, the total H I profile in a beam area centered on the isolated H II region (or regions in the case of 1 and 2, since they are so close) is given. The velocity of all 3 NGC 1533 confirmed isolated H II regions coincide well with H I gas which is bound to and rotating around NGC 1533 (Ryan-Weber et al. 2003a). Are these isolated H II regions progenitors to tidal dwarf galaxies? Since the gas and isolated H II regions are bound to the galaxy, it is likely that the stars formed will also remain bound in the tidal debris. There is certainly a reservoir of gas from which more stars could form, so it is possible in this case that a tidal dwarf galaxy could emerge.

For the other two systems the global H I spectrum is given, since we do not have a synthesis map of HCG 16 and there is no H I detected at the position and velocity of the isolated H II region near ESO 149-G003. The galaxy escape velocity and velocity of the isolated H II region are plotted on each spectrum to determine their kinematic connection. The escape velocity is estimated by $v_{\text{esc}} \sim 1/\sqrt{2}w_{20}\sin(i)$, where w_{20} is the width of the global H I profile at 20% of its height and i is the inclination of the galaxy. No inclination correction is made for HCG 16 since there is more than one galaxy embedded in the H I emission. In HCG 16 the velocity of the isolated H II region sits just inside the escape velocity of the system. It is unclear whether the stars formed will remain bound or whether they will disperse into the intragroup medium. The large difference in velocity between ESO 149-G003 and its candidate isolated H II region suggest the two are not bound. Of course to form a tidal dwarf galaxy, tidal gas is needed, the non-detection of high column density

H_I gas in the vicinity of this H_{II} region candidate rules out this possibility.

4.5. ESO 149-G003: A True Isolated H_{II} Region?

The emission line source near ESO 149-G003 could be a part of an associated extragalactic H_I cloud (although technically H_I clouds don't have optical counterparts). Its H_I mass upper limit of $8 \times 10^5 M_{\odot}$ has implications for the search for extragalactic H_I clouds around other galaxies and in galaxy groups. For example, Zwaan (2001) searched analogues of the Local Group to a 4.5σ limit of $7 \times 10^6 M_{\odot}$ and found no significant extragalactic H_I clouds. This may motivate the search for lower H_I mass extragalactic clouds. This isolated H_{II} region candidate is quite different from the others discussed in this paper. Only one emission line is detected (making the line identification ambiguous), the continuum flux is significantly higher and the apparent velocity difference between ESO 149-G003 and the H_{II} region candidate (assuming the detected emission line is in fact H α , see Figure 5) places the it well outside the escape velocity of ESO 149-G003 (45 km s^{-1}). This kinematic evidence suggests that the source is perhaps a distant emission line galaxy in the field, rather than being associated with ESO 149-G003. Whether the emission line is H α at 995 km s^{-1} or another line at a higher redshift is uncertain. Indeed, we expect a contamination rate of background emission line systems of ~ 1 per SINGG image, based on number statistics from Boroson et al. (1993), Cowie & Hu (1998) and Rhoads et al. (2000). If the emission line is H α , this object holds interesting implications for the census of intergalactic matter. Absorption lines along random lines-of-sight tell us that the IGM is generally clumped spatially and in velocity, and shows a range of densities and metallicities. In future studies isolated H_{II} regions could be used as beacons for star-forming regions of the IGM. This would complement absorption studies along random sight lines and low spatial resolution H_I emission observations of the IGM.

5. Conclusion

The discovery of intergalactic H_{II} regions presented here and in other recent publications provides a small but finite source of enrichment and ionization of the IGM. In two cases the fact that these emission line objects are detected in both H α and [O III] rules out the possibility that they are background emitters. The H α luminosities imply that each isolated H_{II} region is ionized by 4–7 O stars. If these stars have formed *in situ* they represent atypical star formation in a low density environment. The low level of continuum emission from three of four confirmed isolated H_{II} regions suggests the stellar populations are very young and have formed where no stars existed previously. If part of a normal IMF, the corresponding total cluster mass would be $\sim 10^3 M_{\odot}$. In two out of three systems, isolated H_{II} regions are associated with tidal H_I features, providing a reservoir of neutral gas. In one particular system, NGC 1533, the mass, distribution and velocity dispersion of the H_I suggests the rate of star formation ($1.5 \times 10^{-3} M_{\odot} \text{yr}^{-1}$) could be sustained by the collision of clouds. This would result an increase in the metal abundance by $\sim 1 \times 10^{-3}$ solar.

This is the same abundance level as seen in the DLA ‘metallicity floor’ (Prochaska et al. 2003). The amount of intergalactic high column density H_I and rate of collision-triggered intergalactic star formation may have been higher in the past. On-going investigations into the metallicities and underlying stellar population of these and other isolated H_{II} regions in the SINGG images will shed more light on their nature and origin.

6. Acknowledgements

This research has made use of the NASA/IPAC Extragalactic Database (NED). Digitized Sky Survey (DSS) material (UKST/ROE/AAO/STScI) is acknowledged. ERW acknowledges support from an Australia Postgraduate Award. MEP acknowledges support by NASA through Hubble Fellowship grant HST-HF-01132.01 awarded by the Space Telescope Science Institute, which is operated by AURA Inc. under NASA contract NAS 5-26555. MSO acknowledges support from the National Science Foundation Grant AST-0204853. Helpful comments by the referee are gratefully acknowledged.

REFERENCES

Aloisi, A., Savaglio, S., Heckman, T. M., Hoopes, C. G., Leitherer, C., & Sembach, K. R. 2003, ApJ, 595, 760

Ballantyne, D. R., Kerton, C. R., & Martin, P. G. 2000, ApJ, 539, 283

Barnes D. G., et al. 2001, MNRAS, 322, 486

Boroson, T. A., Salzer, J. J., & Trotter, A. 1993, ApJ, 412, 524

Cerviño, M. & Mas-Hesse, J. M. 1994, A&A, 284, 749

Cerviño, M., Valls-Gabaud, D., Luridiana, V., & Mas-Hesse, J. M. 2002, A&A, 381, 51

Chen, H., Lanzetta, K. M., Webb, J. K., & Barcons, X. 2001, ApJ, 559, 654

Christodoulou, D. M., Tohline, J. E., & Keenan, F. P. 1997, ApJ, 486, 810

Clarke, C. J., Bonnell, I. A., & Hillenbrand, L. A. 2000, Protostars and Planets IV, 151

Collins, J. A., Shull, J. M., & Giroux, M. L. 2003, ApJ, 585, 336

Cowie, L. L. & Hu, E. M. 1998, AJ, 115, 1319

Demers, S. & Battinelli, P. 1998, AJ, 115, 154

Duc, P.-A., Brinks, E., Springel, V., Pichardo, B., Weilbacher, P., & Mirabel, I. F. 2000, AJ, 120, 1238

Ferguson, A. M. N., Gallagher, J. S., & Wyse, R. F. G. 1998a, AJ, 116, 673

Ferguson, A. M. N., Wyse, R. F. G., Gallagher, J. S., & Hunter, D. A. 1998b, ApJL, 506, L19

Garcia Vargas, M. L. & Diaz, A. I. 1994, ApJS, 91, 553

Gardiner, L. T. & Noguchi, M. 1996, MNRAS, 278, 191

Gerhard, O., Arnaboldi, M., Freeman, K. C., & Okamura, S. 2002, ApJ, 580, L121

Kennicutt, R. C. 1998, ApJ, 498, 541

Leitherer, C., Schaerer, D., Goldader, J. D., Delgado, R. M. G., Robert, C., Kune, D. F., de Mello, D. F., Devost, D., & Heckman, T. M. 1999, ApJS, 123, 3

Leonard, P. J. T. & Duncan, M. J. 1988, AJ, 96, 222

Maeder, A. 1992, A&A, 264, 105

Martin, C. L. & Kennicutt, R. C. 2001, ApJ, 555, 301

Meyer M., et al. 2003, MNRAS, submitted

Nestor, D. B., Rao, S. M., Turnshek, D. A., & Berk, D. V. 2003, ApJL, accepted

Oey, M. S. & Clarke, C. J. 1998, AJ, 115, 1543

Osterbrock, D. E. 1989, *Astrophysics of gaseous nebulae and active galactic nuclei* (Mill Valley, University Science Books)

Peroux, C., Dessauges-Zavadsky, M., D'Odorico, S., Kim, T. S., & McMahon, R. G. 2003, MNRAS, accepted

Prochaska, J. X., Gawiser, E., Wolfe, A. M., Castro, S., & Djorgovski, S. G. 2003, ApJ, 595, L9

Putman, M. E., Staveley-Smith, L., Freeman, K. C., Gibson, B. K., & Barnes, D. G. 2003, ApJ, 586, 170

Reshetnikov, V. & Combes, F. 1998, A&A, 337, 9

Rhoads, J. E., Malhotra, S., Dey, A., Stern, D., Spinrad, H., & Jannuzi, B. T. 2000, ApJ, 545, L85

Ribeiro, A. L. B., de Carvalho, R. R., Capelato, H. V., & Zepf, S. E. 1998, ApJ, 497, 72

Ryan-Weber, E., Webster, R., & Bekki, K. 2003a, in ASSL Vol. 281: The IGM/Galaxy Connection. The Distribution of Barons at $z=0$, 223

Ryan-Weber, E. V., Webster, R. L., & Staveley-Smith, L. 2003b, MNRAS, 343, 1195

Sakai, S., Kennicutt, R. C., van der Hulst, J. M., & Moss, C. 2002, ApJ, 578, 842

Sato, F., Hasegawa, T., Whiteoak, J. B., & Miyawaki, R. 2000, ApJ, 535, 857

Tonry, J. L., Dressler, A., Blakeslee, J. P., Ajhar, E. A., Fletcher, A. B., Luppino, G. A., Metzger, M. R., & Moore, C. B. 2001, ApJ, 546, 681

Tripp, T. M., Jenkins, E. B., Williger, G. M., Heap, S. R., Bowers, C. W., Danks, A. C., Davé, R., Green, R. F., Gull, T. R., Joseph, C. L., Kaiser, M. E., Lindler, D., Weymann, R. J., & Woodgate, B. E. 2002, ApJ, 575, 697

Vacca, W. D., Garmany, C. D., & Shull, J. M. 1996, ApJ, 460, 914

Verdes-Montenegro, L., Yun, M. S., Williams, B. A., Huchtmeier, W. K., Del Olmo, A., & Perea, J. 2001, A&A, 377, 812

Vollmer, B. & Huchtmeier, W. 2003, A&A, 406, 427

Zhang, Q., Fall, S. M., & Whitmore, B. C. 2001, ApJ, 561, 727

Zwaan, M. A. 2001, MNRAS, 325, 1142

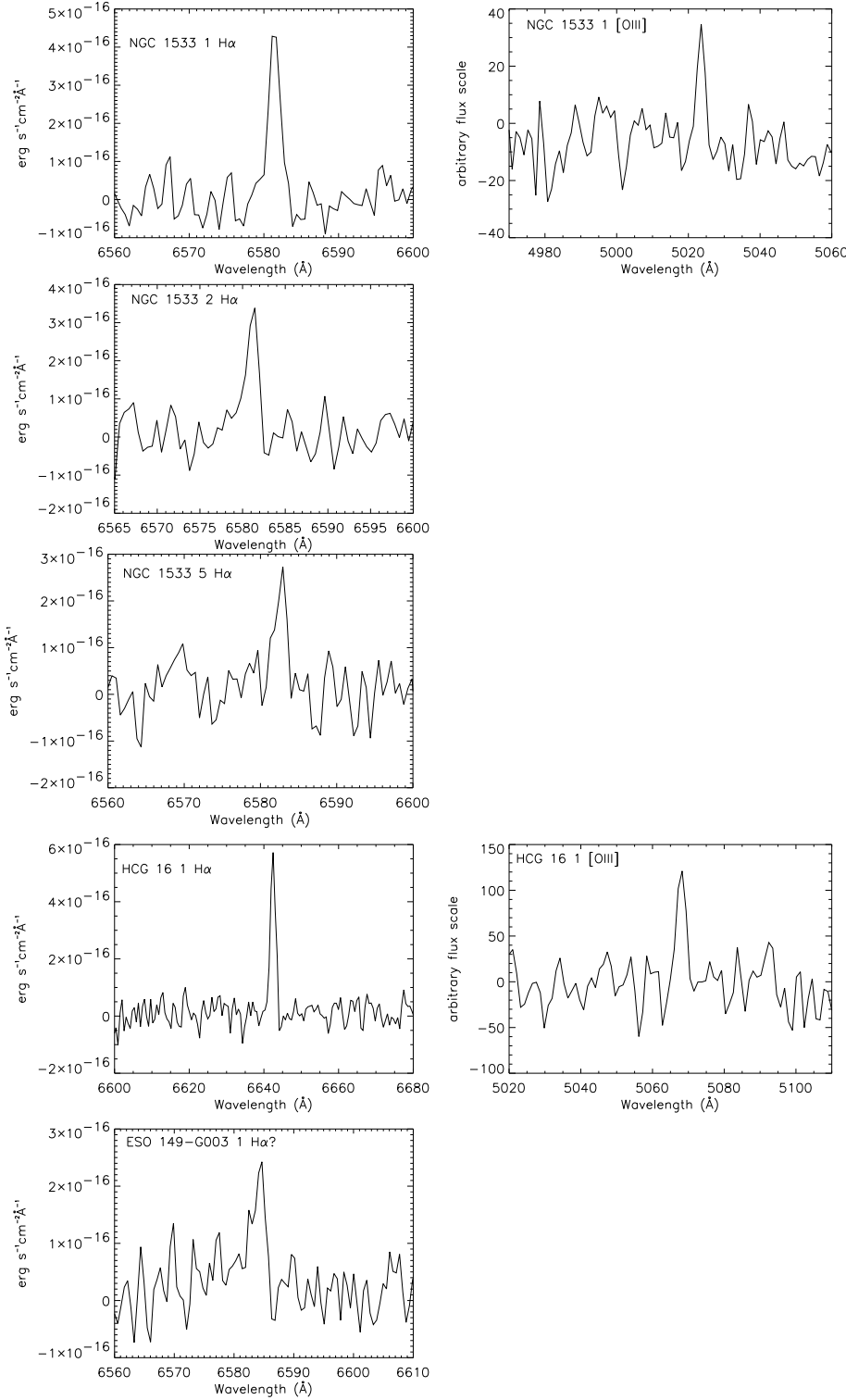


Fig. 1.— Emission lines from detected isolated H II region candidates: H α on the left and [O III] on the right. The H α spectra have been normalised by the integrated H α flux from the SINGG images given in Table 2, corrections for an [N II] component have not been made.

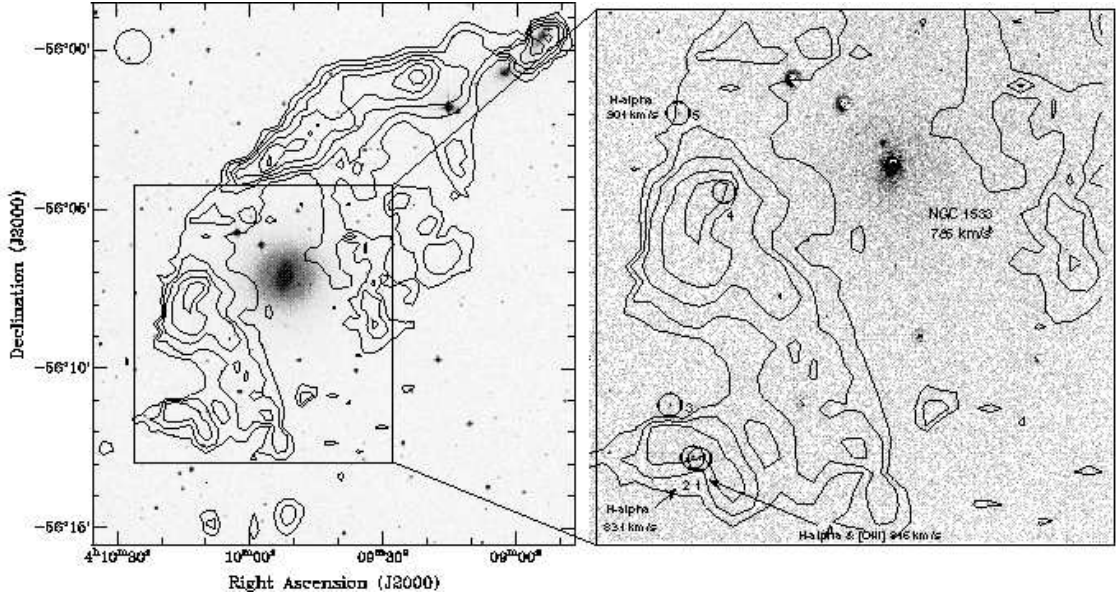


Fig. 2.— NGC 1533: DSS image with ATCA H₁ contours overlaid at 1.6, 2.0, 2.4, 2.8, 3.2, 3.6 and 4×10^{20} cm⁻². The beam is given in the top left corner. The insert shows the continuum subtracted H_α image with the isolated H_{II} regions labelled and H_α velocities given, where available.

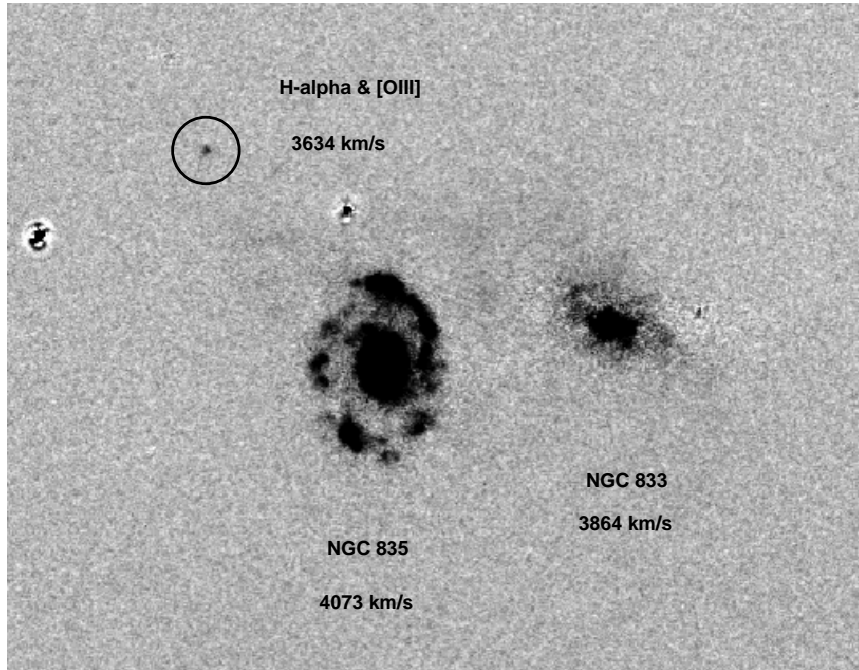


Fig. 3.— HCG 16: Continuum subtracted H_α image with the isolated H_{II} region and two members of the galaxy group labelled. The two other objects in the field are residuals of foreground stars.

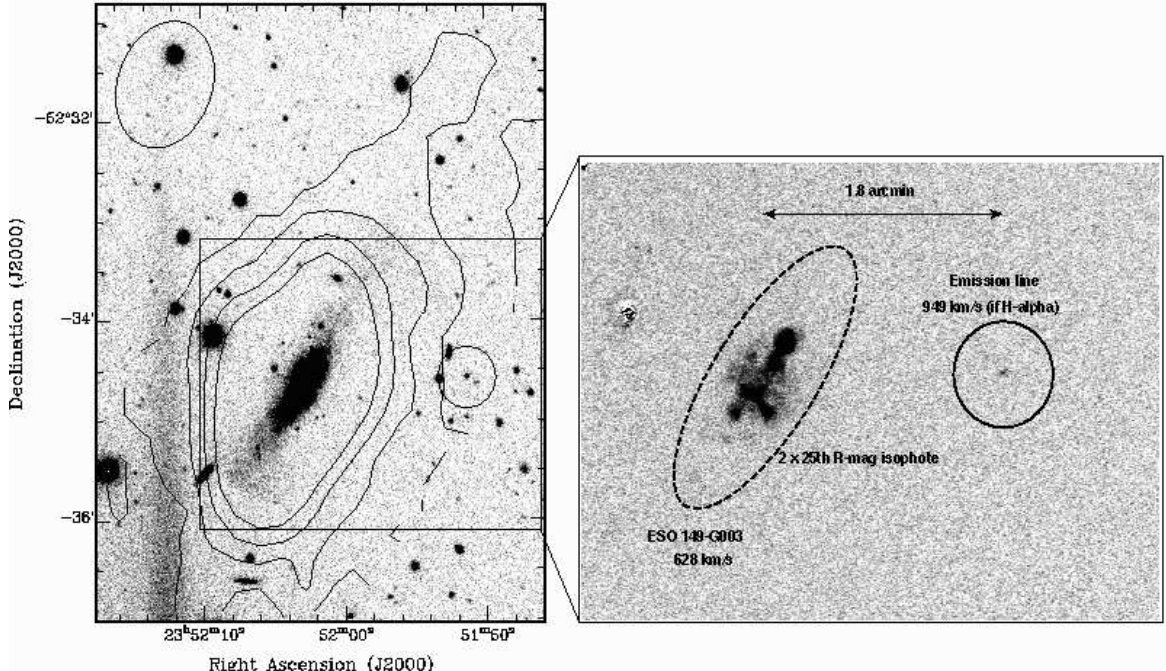


Fig. 4.— ESO 149-G003: R image with ATCA HI contours overlaid at $0.5, 1.0, 1.5$ and $2.0 \times 10^{20} \text{ cm}^{-2}$. The beam is given in the top left corner. The insert shows the continuum subtracted H α image with the isolated HII region candidate and galaxy labelled.

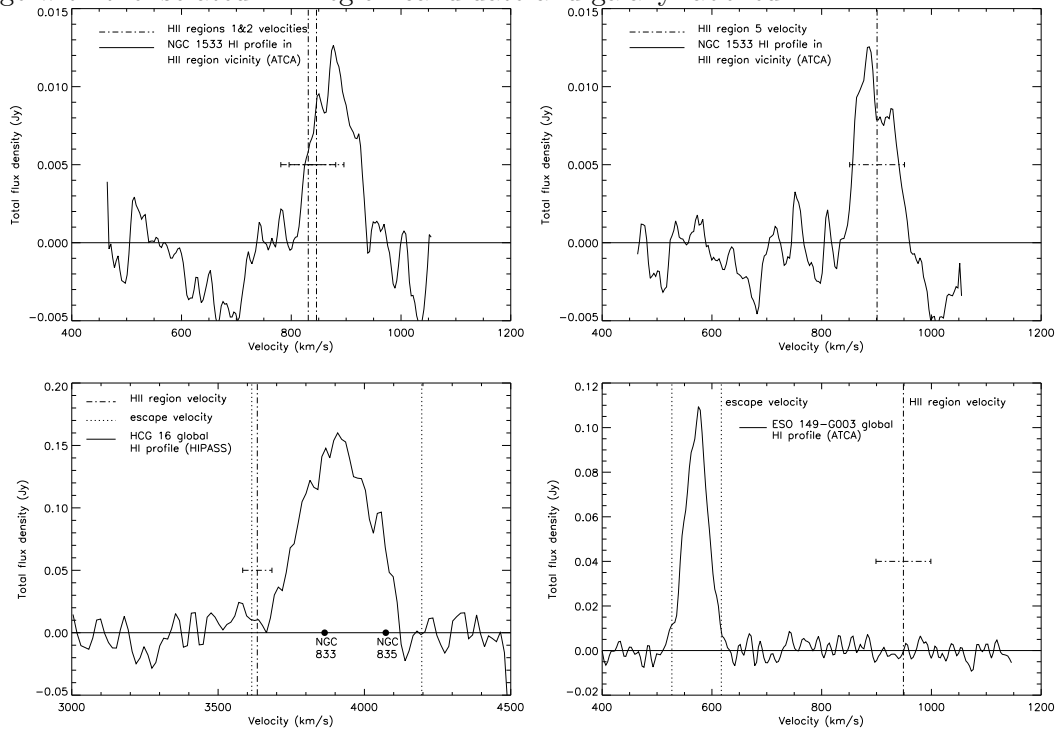


Fig. 5.— HI spectra of the three systems with detected isolated HII regions, the velocities of the HII region candidates are also plotted.

Target Name	Time		Exposure		Seeing		Detection Limit		Surface Brightness Limit	
	R	H α	sec	sec	arcsec	R	H α	R	H α	
						erg s $^{-1}$ cm $^{-2}$ Å $^{-1}$	erg s $^{-1}$ cm $^{-2}$	erg s $^{-1}$ cm $^{-2}$ Å $^{-1}$ arcsec $^{-2}$	erg s $^{-1}$ cm $^{-2}$ arcsec $^{-2}$	
HCG 16	360	1800	1.7			1.08×10^{-18}	1.48×10^{-16}	1.33×10^{-19}		1.51×10^{-17}
ESO 154-G023	360	1800	1.2			9.20×10^{-19}	7.54×10^{-17}	5.57×10^{-19}		1.20×10^{-17}
NGC 1314	360	1800	1.5			9.46×10^{-19}	1.19×10^{-16}	1.05×10^{-19}		9.29×10^{-18}
NGC 1533	480	1800	1.4			9.08×10^{-19}	9.96×10^{-17}	4.99×10^{-19}		1.17×10^{-17}
IC 5052	360	1800	1.4			1.23×10^{-18}	1.11×10^{-16}	2.46×10^{-19}		1.82×10^{-17}
ESO 238-G005	360	1800	1.3			1.01×10^{-18}	1.04×10^{-16}	9.38×10^{-20}		1.20×10^{-17}
ESO 149-G003	360	1800	1.7			1.25×10^{-18}	1.37×10^{-16}	2.72×10^{-19}		1.33×10^{-17}

Table 1: Properties of R and H α SINGG images with isolated H II region candidates. The detection limit is the 5σ point source detection limit. The final two columns give the large scale surface brightness limit calculated as described in the text.

Candidate H II Region Name	m _R AB mag	R Flux erg s $^{-1}$ cm $^{-2}$ Å $^{-1}$	H α Flux erg s $^{-1}$ cm $^{-2}$	EW Å	H α Lum. erg s $^{-1}$	Lines Detected	Velocity km s $^{-1}$
HCG 16 1	> 23.5	< 1.08×10^{-18}	$1.0(\pm 0.05) \times 10^{-15}$	>1764	3.5×10^{38}	H α , [O III]	3634(± 50)
ESO 154-G023 1	21.3 ± 0.1	$7.6(\pm 0.5) \times 10^{-18}$	$3.8(\pm 0.5) \times 10^{-16}$	51	1.3×10^{36}	none	...
NGC 1314 1	21.9 ± 0.1	$4.6(\pm 0.5) \times 10^{-18}$	$1.6(\pm 0.05) \times 10^{-15}$	431	5.2×10^{38}	none	...
NGC 1533 1	23.1 ± 0.3	$1.5(\pm 0.4) \times 10^{-18}$	$1.1(\pm 0.5) \times 10^{-15}$	1113	5.8×10^{37}	H α , [O III]	846(± 50)
NGC 1533 2	22.0 ± 0.1	$4.1(\pm 0.4) \times 10^{-18}$	$6.8(\pm 0.5) \times 10^{-16}$	177	3.6×10^{37}	H α	831(± 50)
NGC 1533 3	22.6 ± 0.2	$2.3(\pm 0.4) \times 10^{-18}$	$6.4(\pm 0.5) \times 10^{-16}$	331	3.4×10^{37}	not obs.	...
NGC 1533 4	22.5 ± 0.2	$2.5(\pm 0.4) \times 10^{-18}$	$5.8(\pm 0.5) \times 10^{-16}$	262	3.1×10^{37}	not obs.	...
NGC 1533 5	> 23.6	< 9.08×10^{-19}	$5.0(\pm 0.5) \times 10^{-16}$	>1658	2.6×10^{37}	H α	901(± 50)
IC 5052 1	22.6 ± 0.3	$2.4(\pm 0.5) \times 10^{-18}$	$3.2(\pm 0.4) \times 10^{-16}$	143	1.3×10^{36}	none	...
IC 5052 2	20.72 ± 0.05	$1.34(\pm 0.05) \times 10^{-17}$	$4.0(\pm 0.4) \times 10^{-16}$	31	1.7×10^{36}	none	...
ESO 238-G005 1	23.1 ± 0.3	$1.5(\pm 0.5) \times 10^{-18}$	$1.4(\pm 0.6) \times 10^{-16}$	102	1.3×10^{36}	none	...
ESO 238-G005 2	> 23.5	< 1.3×10^{-19}	$2.0(\pm 0.6) \times 10^{-16}$	>1778	1.9×10^{36}	none	...
ESO 149-G003 1	20.39 ± 0.03	$1.8(\pm 0.05) \times 10^{-17}$	$6.9(\pm 0.5) \times 10^{-16}$	39	3.5×10^{36}	H α ?	949(± 50)

Table 2: Properties of isolated H II region candidates with DBS spectra. Spectroscopically detected isolated H II regions have velocities listed in the final column. The fluxes and equivalent widths are measured from the SINGG images. In three cases, where the continuum flux is below the detection limit, the upper limit EW is given. The H II regions candidates 3 & 4 of NGC 1533 are included in this and the following table even though no spectra were taken.

Host Galaxy	Velocity km s ⁻¹	Distance Mpc	H II Reg. No.	Separation kpc, R ₂₅	H II Reg. RA	Position Dec	N _{HI} cm ⁻²
HCG 16	3917	53	1	19, 2.0	02:09:28	-10:07:16	...
ESO 154-G023	574	5.3	1	6.0, 3.5	02:56:31	-54:31:35	2.8×10 ¹⁹
NGC 1314	3936	52	1	131, 15.2	03:23:12	-04:15:16	...
NGC 1533	785	21	1	33, 4.0	04:10:13	-56:11:37	2.4×10 ²⁰
NGC 1533	785	21	2	33, 4.0	04:10:14	-56:11:35	2.4×10 ²⁰
NGC 1533	785	21	3	31, 3.8	04:10:17	-56:10:46	9.8×10 ¹⁹
NGC 1533	785	21	4	16, 2.0	04:10:11	-56:07:28	3.2×10 ²⁰
NGC 1533	785	21	5	20, 2.5	04:10:15	-56:06:15	1.5×10 ²⁰
IC 5052	584	5.9	1	8.0, 1.4	20:52:59	-69:12:27	<3.2×10 ¹⁹
IC 5052	584	5.9	2	10, 1.7	20:52:53	-69:16:22	<3.2×10 ¹⁹
ESO 238-G005	706	8.9	1	3.9, 30	22:22:33	-48:25:42	2.4×10 ²⁰
ESO 238-G005	706	8.9	2	11, 84	22:22:42	-48:27:53	<3.2×10 ¹⁹
ESO 149-G003	576(628) ^a	6.5	1	3.4, 5.2	23:51:51	-52:34:34	<3.2×10 ¹⁹

Table 3: Isolated H II region candidates with DBS spectra. The velocity is the heliocentric velocity of the host galaxy measured by HIPASS. The distance given is to the host galaxy, HCG 16 uses the mean recessional velocity from Ribeiro et al. (1998), NGC 1533 uses the distance from Tonry et al. (2001) and all other galaxies use the local group corrected velocity. The projected separation in kpc (to the optical centre) is calculated using this distance. The projected separation is also calculated as a fraction of R₂₅, the major axis of the isophote at $\mu_R = 25\text{mag arcsec}^{-2}$. The H I column densities are measured from ATCA maps, at the position of the H II region candidates, where available.

^aVelocity of the H α line in the galaxy measured from the same long-slit spectrum as the isolated H II region is 628 (± 50) km s⁻¹.